

The 3D protein of duck hepatitis A virus type 1 binds to a viral genomic 3' UTR and shows RNA-dependent RNA polymerase activity

Yu Zhang^{1,2} · Qianda Cao^{1,2} · Mingshu Wang^{1,2,3} · Renyong Jia^{1,2,3} · Shun Chen^{1,2,3} · Dekang Zhu^{2,3} · Mafeng Liu^{1,2,3} · Kunfeng Sun^{1,2,3} · Qiao Yang^{1,2,3} · Ying Wu^{1,2,3} · Xinxin Zhao^{1,2,3} · Xiaoyue Chen^{1,2} · Anchun Cheng^{1,2,3}

Received: 18 March 2017 / Accepted: 5 June 2017 / Published online: 9 June 2017
© Springer Science+Business Media, LLC 2017

Abstract To explore the RNA-dependent RNA polymerase (RdRP) function of the 3D protein of duck hepatitis A virus type 1 (DHAV-1), the gene was cloned into the pET-32a(+) vector for prokaryotic expression. The 3' untranslated region (3' UTR) of DHAV-1 together with a T7 promoter was cloned into the pMD19-T vector for in vitro transcription of 3' UTR RNA, which was further used as a template in RNA-dependent RNA polymerization. In this study, three methods were applied to analyze the RdRP function of the 3D protein: (1) ammonium molybdate spectrophotometry to detect pyrophosphate produced during polymerization; (2) quantitative reverse transcription PCR (RT-qPCR) to investigate the changes in RNA quantity during polymerization; and (3) electrophoresis mobility shift assay to examine the interaction between the 3D protein and 3' UTR. The results showed the 3D protein was successfully expressed in bacteria culture supernatant in a soluble form, which could be purified by affinity chromatography. In 3D enzymatic

activity assays, pyrophosphate and RNA were produced, the amounts of which increased based on approximative kinetics, and binding of the 3D protein to the 3' UTR was observed. These results indicate that prokaryotically expressed soluble DHAV-13D protein can bind to a viral genomic 3' UTR and exhibit RdRP activity.

Keywords DHAV-1 · 3D protein · RdRP activity · 3' UTR

Introduction

Duck viral hepatitis (DVH) is an acute, highly deadly and contagious disease of ducklings first reported in America in 1949 [1, 2]. DVH is caused by three serotypes of the duck hepatitis virus: duck hepatitis A virus (DHAV), duck astrovirus type 1 (DAstV-1), and duck astrovirus 2 (DAstV-2), earlier named DHV-I, DHV-II, and DHV-III, respectively [3–7]. According to the latest version of *ICTV (International Committee on Taxonomy of Viruses) Report on Virus Taxonomy*, DHAV has been renamed Avihepatovirus A and classified as the only member of the *Avihepatovirus* genus in the *Picornaviridae* family [8]. DHAV has been divided into three genotypes, DHAV-1, DHAV-2, and DHAV-3, according to phylogenetic analysis [7, 9]. DHAV-1 is the most common and harmful type to the duck industry [10–12].

The picornavirus genome consists of a single-stranded, positive-sense RNA molecule that encodes four structural proteins (VP1, VP2, VP3, and VP4) and seven non-structural proteins (2A, 2B, 2C, 3A, 3B, 3C, and 3D). However, DHAV has a unique genome structure that encodes 12 mature proteins, including structural (VP0, VP1, and VP3) and non-structural (2A1, 2A2, 2A3, 2B, 2C, 3A, 3B, 3C, and 3D) proteins [9, 13, 14]. 3D is the most important non-

Edited by Joachim Jakob Bugert.

✉ Mingshu Wang
mshwang@163.com

✉ Anchun Cheng
chenganchun@vip.163.com

- ¹ Institute of Preventive Veterinary Medicine, Sichuan Agricultural University, Chengdu 611130, People's Republic of China
- ² Key Laboratory of Animal Disease and Human Health of Sichuan Province, Sichuan Agricultural University, Chengdu 611130, People's Republic of China
- ³ Research Center of Avian Disease, College of Veterinary Medicine, Sichuan Agricultural University, Chengdu 611130, People's Republic of China

structural picornavirus protein [15], and it possesses strong immunogenicity. It has been reported that transgenic FVB mice carrying the TMEV 3D gene show varying degrees of resistance to Theiler's murine encephalomyelitis virus (TMEV), encephalomyocarditis virus (EMCV), and pseudorabies virus (PRV) of the *Herpesviridae* family as well as vesicular stomatitis virus (VSV) of the *Rhabdoviridae* family [16]. Enzyme-linked immunosorbent assay (ELISA) methods based on eukaryotically and prokaryotically expressed foot-and-mouth disease virus (FMDV) 3D protein have been established to detect levels of anti-FMDV antibodies [17, 18]. In addition to possessing immunological properties, the 3D protein plays an important role in the replication of picornavirus by acting as an RNA-dependent RNA polymerase (RdRP). RdRPs recognize and bind to the 3' untranslated region (UTR) of viral positive-stranded RNA and synthesize the negative strand; thus, numerous positive-stranded RNAs will be synthesized by RdRP using the negative strand as a template [19–22]. As a key enzyme in the replication of positive-stranded RNA viruses, RdRP is a popular target for antiviral drug research.

The RdRP activity of picornavirus 3D proteins has been extensively studied in FMDV and poliovirus (PV) [23–27]. However, studies to date on the DHAV 3D protein are limited in its molecular biology characters [7, 9, 28–30] and epidemiological [11] analyses, PCR-based detection methods [31–36], and siRNA antiviral studies targeting 3D genes [37]. In contrast, the RdRP activity of the DHAV 3D protein has not yet been reported. According to bioinformatic analysis, DHAV-1 3D gene is 1359 bp long, and encodes 453 peptides and has 6 N-glycosylation sites. And DHAV-1 is evolutionary close to DHAV-3, DHV1-04G and DHV1-90D in the genus *Avihepatovirus* based on the amino sequences of 3D proteins from *Picornaviridae* [32, 33]. In this study, the 3D protein of DHAV-1 was prokaryotically expressed. And the DHAV-1 3' UTR, for use as an RNA template, was isolated by in vitro transcription. Multiple methods were then utilized to detect the RdRP activity of the DHAV-1 3D protein. The results could be significant for research into the viral replication mechanism and for anti-DHAV-1 drugs that target the 3D protein.

Materials and methods

Virus, vectors, and duck serum and embryos

The DHAV-1 H strain (GenBank Accession No. JQ301467) and *Escherichia coli* (*E. coli*) strains DH5 α , BL21, PLYS and Rosetta were provided by the Research Center of Avian Disease, Sichuan Agricultural University.

Healthy duck embryos were obtained from a farm in Yaan, China. The pET-32a(+) vector was obtained from Novagen (Germany).

Reagents

RNAiso Plus, PrimeScriptTM RT-PCR Kit, PrimeSTAR[®] Max DNA Polymerase, SYBR[®] Premix Ex TaqTM II (Tli RNaseH Plus), pJET-1.2 PCR Cloning Kit, T-Vector pMDTM19 (Simple), DNA Ligation Kit Ver.2.1, DL2000 DNA Marker, DL15,000 DNA Marker, RNA Marker RL1000, endonucleases KpnI, XhoI and EcoRI were obtained from TaKaRa (China). RNasin was obtained from TIANGEN (China). Inorganic pyrophosphatase (PPase) and Phosphate Colorimetric Assay Kit were obtained from Sigma (United States). ScriptMAX Thermo T7 Transcription Kit was obtained from ToYoBo (Japan). The oligo(dT)₁₂₋₁₈ primer, NTP Mixture, PierceTM RNA 3' End Biotinylation Kit and LightShift[®] Chemiluminescent RNA EMSA Kit were obtained from ThermoFisher Scientific (United States). Amersham HybondTM-N+ positively charged nylon membrane was obtained from GE Healthcare (United States). All custom oligonucleotides were synthesized by Invitrogen (China). The other chemicals were all of analytical grade.

Amplification of the DHAV-1 3D gene and expression vector construction

Primers 3D-F (5'-GGGGTACCGATCAAGGAAAGTAGTGAGCAAG-3') and 3D-R (5'-ACGCCTCGAGTCAGATCATCATGCAAGCTGT-3') were used for reverse transcription and amplification of the 3D gene; viral RNA extracted from allantoic fluid of duck embryos inoculated with DHAV-1 was used as the template. The PCR product was ligated into vector pJET-1.2 to generate pJET-1.2/DHAV-H-3D, which was subsequently digested with KpnI and XhoI and cloned into pET-32a(+), to generate pET-32a(+)/DHAV-H-3D. The two recombinant plasmids were confirmed by PCR, endonuclease digestion, and sequencing.

Expression and purification of the 3D protein

The recombinant plasmid pET-32a(+)/DHAV-H-3D was transformed into *E. coli* for prokaryotic expression of the 3D protein. The protein was identified by sodium dodecyl sulfate-polyacrylamide gel electrophoresis (SDS-PAGE) and western blotting using the serum of DHAV-1-infected ducks. To obtain supernatant with abundant soluble 3D protein, we successively screened and optimized the bacterial expression strain, the concentration of isopropyl β -D-1-thiogalactopyranoside (IPTG), and the induction time

Table 1 Standard binding reactions for electrophoresis mobility shift assays

Component	Reaction			
	1	2	3	4
10× binding buffer	2 µL	2 µL	2 µL	2 µL
tRNA (10 mg/mL)	1 µL	1 µL	1 µL	1 µL
50% glycerol	2 µL	2 µL	2 µL	2 µL
KCl (2 M)	1 µL	1 µL	1 µL	1 µL
MgCl ₂ (1 M)	2 µL	2 µL	2 µL	2 µL
BSA	–	–	–	10 µg
Purified 3D protein	10 µg	–	10 µg	–
Biotin-labeled 3' UTR	–	2 nM	2 nM	2 nM
Nuclease-free water	up to 20 µL			

and temperature. First, three *E. coli* strains (BL21, PLYS and Rosetta) were screened to determine the optimal strain under the following conditions: induction with 0.8 mM IPTG for 6 h at 25 °C. To determine the optimal IPTG concentration, serial concentrations (0.2, 0.4, 0.6, 0.8, and 1.0 mM) were then used to induce protein expression for 6 h at 25 °C using the optimal *E. coli* strain. To determine the optimal induction time, different times (4, 6, 8, 10, and 12 h) were next evaluated at 25 °C using 0.8 mM IPTG and the optimal *E. coli* strain. Finally, to determine the optimal induction temperature, different temperatures (39, 37, 35, 30, 25, and 20 °C) were assessed with the previously ascertained optimal induction time, IPTG concentration and *E. coli* strain. The 3D protein was strongly expressed and purified by Ni²⁺-NTA (nitrilotriacetic acid) affinity chromatography using BioLogic DuoFlow™ System (Bio-Rad). The purified protein was concentrated by ultra-filtration and examined by SDS-PAGE. Furthermore, the supernatant (crude protein without purification) was combined in 20 mM Tris-HCl, and the concentrations of the 3D protein in both the purified and crude samples were

determined using a NanoDrop 2000 Spectrophotometer (Thermo Scientific).

Cloning, in vitro transcription, and purification of the DHAV-1 3' UTR

Primers 3' UTR-F (5'-TAATACGACTCACTATAGA CTGTTGGTCCGCAGATACC-3') and 3' UTR-R (5'-GAATTCTTTTTTTTTTTTTTTTTTTTTTTTATGGTAGGGTA GGAATAGT-3') were used for reverse transcription and amplification of the genomic 3' UTR of DHAV-1. The PCR products were cloned into vector pMD19-T (Simple) to generate pMD19-T/DHAV-X-3' UTR, which was subsequently digested by EcoRI. The digested product was purified and used as the template for in vitro transcription of DHAV-1 3' UTR RNA following the ScriptMAX Thermo T7 Transcription Kit manufacturer's instructions. The RNA transcripts were extracted using RNAiso Plus, and purity was determined by 5% agarose gel electrophoresis.

Ammonium molybdate spectrophotometry

To apply ammonium molybdate spectrophotometry, an A₆₅₀-phosphate concentration standard curve was first prepared following the Phosphate Colorimetric Assay Kit manufacturer's instructions. The RdRP activity assay was carried out in a series of 200-µL reactions containing 25 mM (final concentration, hereafter as well) Tris-HCl (pH 7.8), 2.5 mM MgCl₂, 4 mM dithiothreitol (DTT), 20 U/mL RNasin, 1 µM Oligo(dT)_{12–18} primer, 200 µM NTPs, 3 µM PPase, 0.5 µM 3' UTR RNA, and 2 µM purified or crude 3D protein. An equal volume of RNase-free water instead of the 3D protein was used as negative control group. Bovine serum albumin (BSA), the molecular weight of which approximates that of the recombinant 3D protein (~66.4 kDa), was applied to act as an unrelated protein control. RNA polymerization reactions were

Table 2 Gradient and competitive binding reactions for electrophoresis mobility shift assays

Component	Reaction						
	1	2	3	4	5	6	7
10× binding buffer	2 µL	2 µL	2 µL	2 µL	2 µL	2 µL	2 µL
tRNA (10 mg/mL)	1 µL	1 µL	1 µL	1 µL	1 µL	1 µL	1 µL
50% glycerol	2 µL	2 µL	2 µL	2 µL	2 µL	2 µL	2 µL
KCl (2 M)	1 µL	1 µL	1 µL	1 µL	1 µL	1 µL	1 µL
MgCl ₂ (1 M)	2 µL	2 µL	2 µL	2 µL	2 µL	2 µL	2 µL
Purified 3D protein	40 µg	20 µg	10 µg	5 µg	2.5 µg	10 µg	10 µg
Biotin-labeled 3' UTR	2 nM	2 nM	2 nM	2 nM	2 nM	0.5 nM	1 nM
Unlabeled 3' UTR	–	–	–	–	–	1.5 nM	1 nM
Nuclease-free water	up to 20 µL						

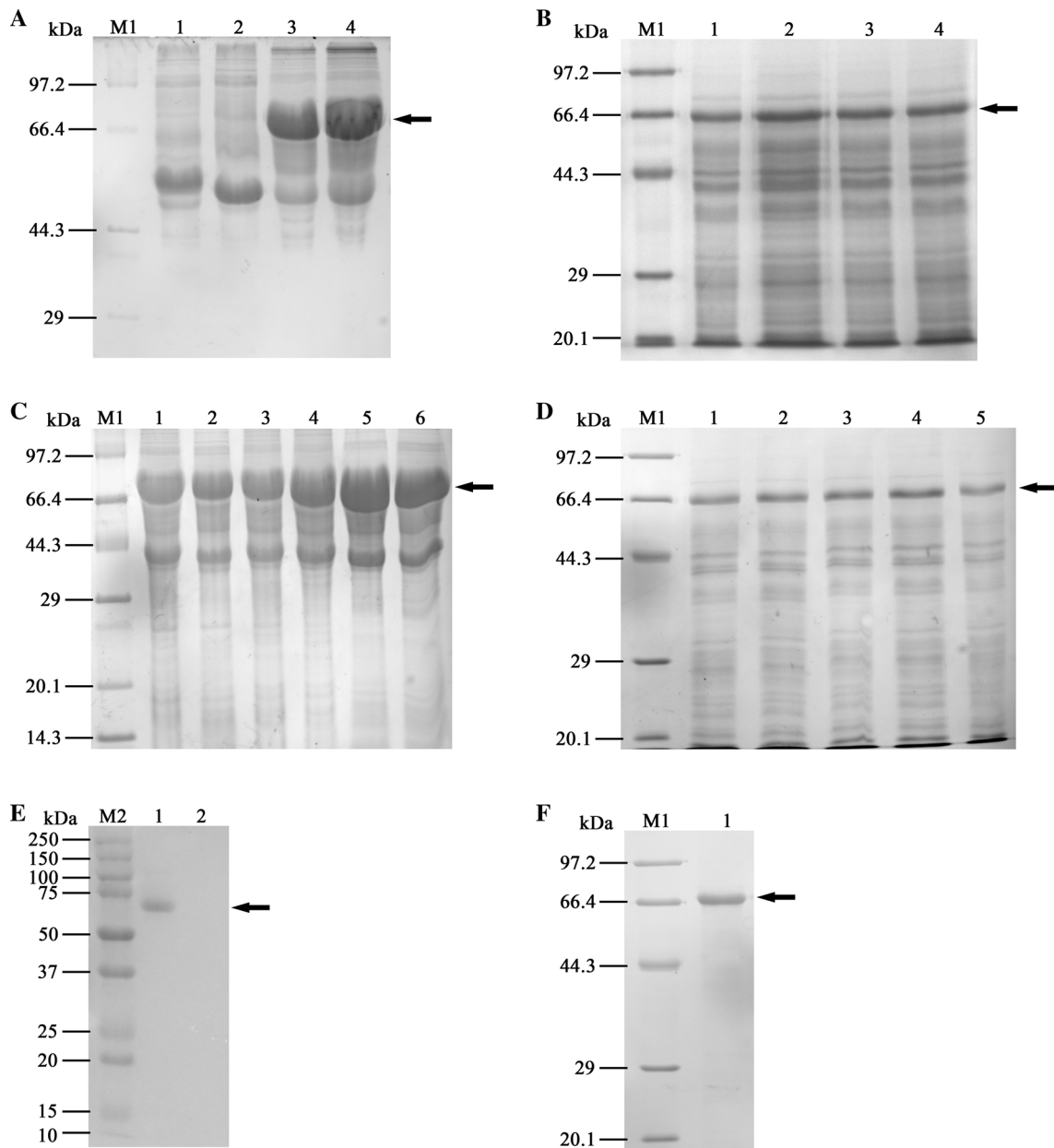


Fig. 1 Optimizing expression conditions, identifying, and purifying of the 3D protein. **a** Different strains of host bacteria were screened. *Lane 1* shows the expression product of the pET-32a(+) vector in BL21 as control, and *lanes 2–4* show the expression products of recombinant pET-32a(+)/DHAV-H-3D in Rosetta, BL21, and PLYS cells, respectively. **b** The induction times for 3D protein expression. *Lanes 1–5* show protein expression in 12, 10, 8, 6 and 4 induction hours, respectively. **c** The induction temperature for 3D protein expression. *Lanes 1–6* show the products using PLYS at 39,

performed at 30 °C for 15, 30, 45, 60, 75, 90, 105, and 120 min, and four replicates were included for each reaction time. The reactions were terminated by addition of 2 μ L 0.5 M EDTA (pH 8.0). The A_{650} values of all reactions were measured using an iMarkTM Microplate Reader (Bio-Rad).

37, 35, 30, 25 and 20 °C, respectively. **d** Induction IPTG concentrations. *Lanes 1–5* show the products using PLYS with 0.2, 0.4, 0.6, 0.8 and 1.0 mM IPTG, respectively. **e** Western blot identification of the 3D protein. *Lane 1* shows the 3D protein. **f** Purified 3D protein detection by SDS-PAGE. *Lane 1* and 2 show the purified 3D protein and the empty vector expression respectively. M1 and M2 represent the non-stained and pre-stained protein standards respectively. The arrow shows the target bands

Quantitative reverse transcription PCR

Primers Q-3' UTR-F (5'-TGTTGGTCCGCAGATAC-3') and Q-3' UTR-R (5'-GTCAAGCTGGGAGGTGT-3') were used to prepare the standard curve and quantify the samples. First, a tenfold gradient dilution of the plasmid pMD19-T/

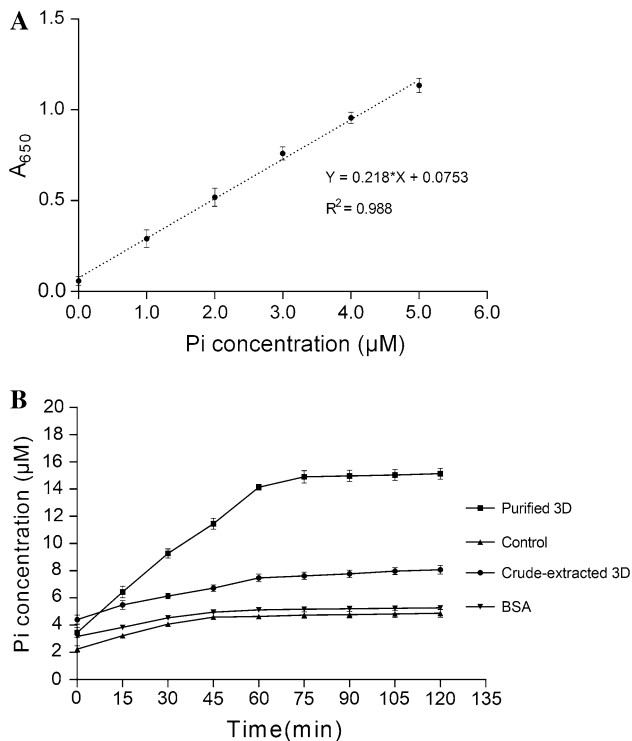


Fig. 2 RdRP activity of the 3D protein by ammonium molybdate spectrophotometry. **a** A standard curve of the phosphate concentration determined at A_{650} . The standard curve was constructed following the manufacturer's instructions of Phosphate Colorimetric Assay Kit. **b** Results of ammonium molybdate spectrophotometry. A_{650} of RNA polymerization reactions was detected at each time point and converted to a phosphate concentration using the standard curve

DHAV-X- 3' UTR was prepared as standards, and four replicates were included for each dilution. The diluted standards were quantified following the SYBR[®] Premix Ex Taq[™] II (Tli RNaseH Plus) manufacturer's instructions to generate the standard curve. The RdRP reactions for RT-qPCR were prepared according to the reactions of ammonium molybdate spectrophotometry. Once the reactions reached the corresponding time points, the RNA in the polymerization reactions was extracted using RNAiso Plus for reverse transcription; the amount of transcribed cDNA was quantified and converted into copy number.

Electrophoresis mobility shift assay

The prepared 3' UTR RNA was labeled with biotin and extracted using RNA 3' End Biotinylation Kit and RNAiso Plus, respectively, following the manufacturers' instructions. Following the manufacturer's instructions of LightShift[®] Chemiluminescent RNA EMSA Kit, a native 5% polyacrylamide gel (8 × 8 × 0.1 cm) was prepared and pre-electrophoresed in 0.5× TBE for 30–60 min at a voltage of 100 V. Series of standard binding reactions were prepared as shown in Table 1, with tRNA as the non-

specific competitor and BSA as an unrelated protein control (reaction 4). Reactions without the 3D protein (reaction 1) or the biotin-labeled DHAV-1 3' UTR (reaction 2) were included as negative controls. To further identify the concentration dependency of the binding ability, another series of gradient and competitive binding reactions were prepared. As shown in Table 2, gradient amount of 3D proteins and biotin-labeled 3' UTR were respectively added into the reactions, and unlabeled 3' UTR was applied as the specific competitor. The reactions were incubated at room temperature for 20–30 min and electrophoresed. Once the bromophenol blue dye in the samples has migrated approximately 3/4 down the length of the gel, the RNA on the gel was electrophoretically transferred to a positively charged nylon membrane in 0.5× TBE and crosslinked at 120 mJ/cm² using a UV-light crosslinking instrument. The biotin-labeled RNA was detected by chemiluminescence using ChemiDoc[™] MP System (Bio-Rad).

Results

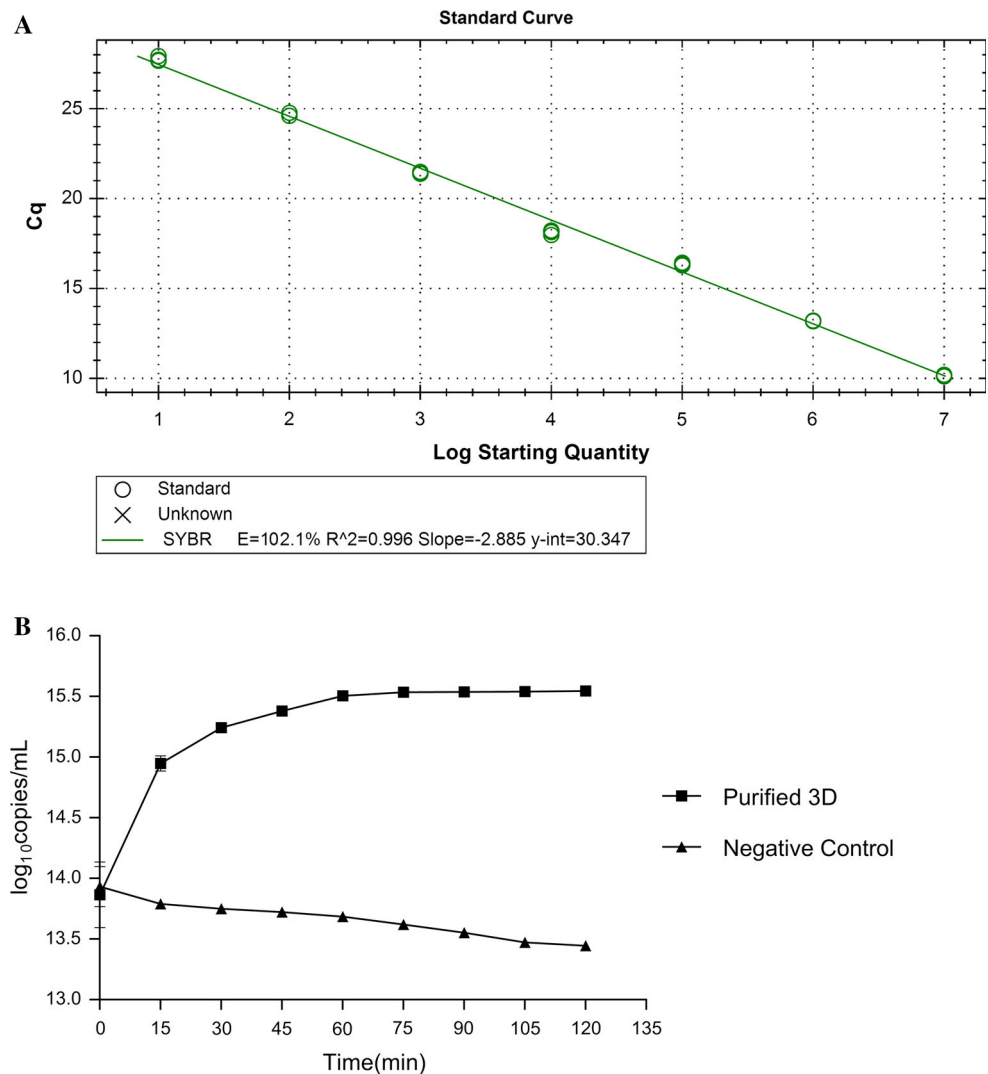
Expression and purification of DHAV-1 3D protein

To obtain abundant soluble 3D protein, the DHAV-1 3D gene was cloned into the pET-32a(+) vector and fused to Trx and His tags. The induction conditions, including the *E. coli* strain, concentration of IPTG, temperature, and time, were successively optimized. As shown in Fig. 1, the target band appears at approximately 66.4 kDa by SDS-PAGE. Moreover, the 3D protein was only found in the supernatant of *E. coli* strains BL21 and PLysS cultures, after grayscale analysis using ImageJ2x software (freeware available at <http://rsb.info.nih.gov/ij/>), the intensity of the expected band in lane of PLysS is 1.70 times that of lane of BL21 (data not shown), thus PLysS exhibiting more robust expression (Fig. 1a). The amount of protein expressed increased as the induction temperature decreased (Fig. 1c). Conversely, the induction time (Fig. 1b) and IPTG concentration (Fig. 1d) did not significantly affect the yield of the desired protein. Thus, the selected optimal induction conditions were 0.8 mM IPTG for 6 h at 25 °C. Western blot analysis showed that the expressed protein reacted strongly with DHAV-1-infected duck serum (Fig. 1e), indicating that the soluble Trx-fused 3D protein was successfully expressed in the supernatant. By fusing with a His tag, the recombinant protein was readily purified by Ni²⁺-NTA affinity chromatography (Fig. 1f).

RdRP activity identification of the 3D protein

Ammonium molybdate spectrophotometry was firstly used to detect RdRP activity of the recombinant 3D protein, an

Fig. 3 RdRP activity of the 3D protein using quantitative reverse transcription PCR (RT-qPCR). **a** Standard curve for quantification of the 3' UTR. The standard curve for RT-qPCR was constructed following the manufacturer's instructions for SYBR® Premix Ex Taq™ II (Tli RNaseH Plus). **b** The change of RNA content in the reaction system. RNA generated from reactions at each time point was extracted and transcribed, and quantification of the transcripts was determined and converted to \log_{10} copies



A_{650} -phosphate concentration curve (Fig. 2a) was constructed, and the RdRP activity of the purified and crude 3D proteins were determined (Fig. 2b). Compared with the negative control groups, the content of phosphoric acid in reactions including the purified and crude 3D proteins increased within the first 75 min, indicating that the enzymatic activity of the 3D protein indeed produced pyrophosphate. The curve of the crude 3D is little higher than that of the controls but much lower than that of the purified, suggesting that the crude extract hardly showed the activity. In addition, when the reaction time reached 75 min, the phosphoric acid content of the reactions containing purified 3D protein increased gradually, suggesting that the reaction had reached a plateau, most likely due to substrate degradation and depletion. Interestingly, the phosphoric acid content of the negative control groups also increased slightly during the first 45 min, may indicate that the solubility of the substrate in the reaction gradually changes.

Quantitative RT-PCR was applied to further quantify the enzymatic activity of the 3D protein. A standard curve was first established (Fig. 3a). As shown in Fig. 3b, in the first 90 min, the amount of RNA at the end of reactions in samples in which the 3D protein was added was significantly higher compared with the negative control group. This result indicates that RNA is generated in the reaction system. In addition, it can be easily observed that the increasing trend of the amount of RNA conforms to the ammonium molybdate spectrophotometry results (Fig. 2b). In contrast, the amount of RNA in the negative control group reactions gradually decreased, potentially caused by RNA degradation.

The binding ability of 3D protein to the 3' UTR

To further verify the function of the prokaryotically expressed soluble DHAV-1 3D protein, its ability to bind to the 3' UTR was examined by EMSA. As shown in Fig. 4a,

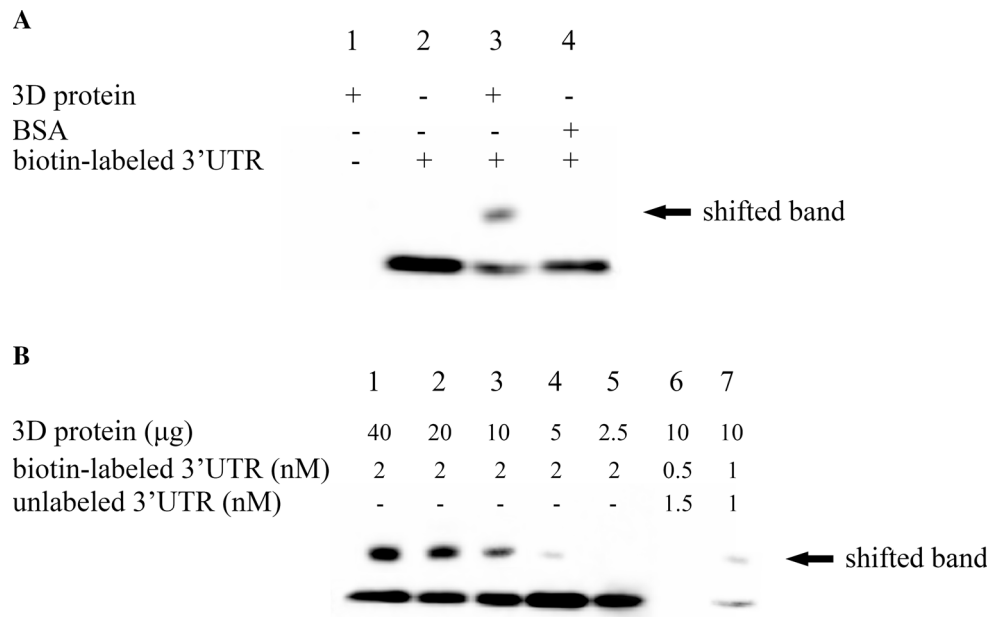


Fig. 4 Identification of the binding between DHAV-1 3D protein and DHAV-1 3' UTR by EMSA. **a** Result of the standard EMSA. *Lanes 1* and *2*, reactions without the 3D protein (reaction 1) or biotin-labeled DHAV-1 3' UTR as negative controls. *Lane 3*, biotin-labeled 3' UTR and 3D protein without non-labeled 3' UTR were both added to detect the binding ability of the 3D protein to the 3' UTR. *Lane 4*, irrelevant

protein control, in which BSA was used instead of the 3D protein. The arrow shows the shifted band. **b** Result of the gradient and competitive EMSA. Gradient amount of 3D proteins (*lanes 1* to *5*) and biotin-labeled 3' UTR (*lane 3*, *6* and *7*) were respectively added into the reactions to investigate the concentration dependency of the binding

no shifted band was observed in the negative control groups (*lanes 1* and *2*) and the irrelevant protein control group (*lane 4*). Conversely, in reactions containing the 3D protein, an obvious shifted band can be observed. Furthermore, as Fig. 4b shows, adding increasing amount of 3D protein resulted in stronger shifted bands (*lanes 1–5*). In addition, when unlabeled 3' UTR competes with the biotin-labeled to bind to 3D protein, the shifted band gets weaker, and adding excessive amount of unlabeled 3' UTR resulted in loss of binding (*lanes 3*, *6* and *7*). These results evidently indicated that the DHAV-1 3D protein strongly bound to the 3' UTR.

Discussion

Bioinformatic analysis suggests that the DHAV-1 3D protein possesses RdRP activity [29], but this finding has not yet been confirmed by experimental analysis. To further understand the structure and function of the protein, isolation of DHAV-1 3D with high purity and yield is needed. Although expression in *E. coli* is widely used to produce proteins for functional analyses, many proteins form insoluble inclusion bodies, which are inactive aggregates. In contrast, soluble fusion proteins more closely adopt the natural conformation of a protein, and such

recombinant proteins have been shown to have strong biological activity [38]. Therefore, the key to functional studies of prokaryotically expressed proteins is to isolate a soluble protein of interest. In this study, to obtain soluble DHAV-1 3D protein, the 3D gene was fused to Trx and His tags, which are utilized for soluble expression and purification, respectively. The Trx (thioredoxin) tag has a molecular weight of approximately 12 kDa. Many studies have shown that Trx tags can limit the formation of inclusion bodies [39, 40], and fusion of the Trx tag with a target protein can effectively improve expression and solubility [41–43], with little effect on the immunogenicity [44–46] or catalytic activity of the target protein [47–51]. In addition, the His tag is thought to have negligible or near negligible effects on target proteins [52]. The application of Trx and His tags play important roles in RdRP activity of the recombinant 3D protein in this study.

Ammonium molybdate spectrophotometry and quantitative RT-PCR were successively applied to detect the RdRP activity of DHAV-1 3D protein. Ammonium molybdate spectrophotometry detected the phosphoric acid (Pi), which was produced in the RdRP reaction system in the presence of pyrophosphatase (PPase). The increasing amount of Pi suggested the RdRP activity of DHAV-1 3D protein, and the activity kinetics corresponded to that of FMDV and PV 3D proteins [24, 27]. In this study, the

purified 3D protein behaved strong RdRP activity while the crude extract hardly showed the activity, which may result from that the concentration of 3D protein in the purified will be much higher than that in the crude extract. Quantitative RT-PCR method directly detected the increase of the polymerized RNA, and the increasing trend conforms to the ammonium molybdate spectrophotometry results, which further proved the RdRP activity of 3D protein. In summary, the above-mentioned two methods detected the formation of pyrophosphate and RNA in 3D reactions, thus it is reasonable to conclude that the prokaryotically expressed soluble 3D protein indeed possesses RdRP activity.

According to the EMSA results, DHAV-1 3D protein shows excellent ability to bind to the genomic 3' UTR, which further confirms its biological activity. This result is consistent with the mechanism used by single-stranded, positive-strand RNA virus RdRP to bind to genomic 3' UTRs and initiate the synthesis of negative-strand RNA [19–22]. The picornavirus EMCV 3D protein also binds to its 3' UTR, and the U-rich region and poly(A) are necessary for this binding; these two regions may generate the binding site by forming a pseudoknot structure [53, 54]. However, the structure of the 3' UTR binding site to which the DHAV-1 3D protein binds remains to be studied.

This study reports the prokaryotic expression, purification, and characterization of the RNA-dependent RNA polymerase activity of soluble DHAV-1 3D protein. Recombinant proteins were obtained with high purity using affinity chromatography. In 3D protein polymerization reactions, the generation of PPi and RNA was detected by ammonium molybdate spectrophotometry and RT-qPCR, respectively. EMSA results demonstrated that the 3D protein binds to the viral genomic 3' UTR. The successful expression and purification of the 3D protein from *E. coli* are significant for research into the biochemical and structural properties of the 3D protein.

Acknowledgements The research was supported by the National Natural Science Foundation of China (Grant No. 31472223), the China Agricultural Research System (CARS-43-8), and the Integration and Special Fund for Key Laboratory of Animal Disease and Human Health of Sichuan Province (2016JPT0004).

Statement of author contributions YZ cloned plasmids, purified the protein, performed the enzymatic activity detection and wrote the manuscript. QC cloned plasmids and expressed and identified the protein. MW and AC designed the experiments. RJ, SC, DZ, ML, KS, QY, YW, XZ, and XC helped with proofreading of the manuscript.

Conflict of interest The authors declare that they have no conflict of interest.

Ethical approval This article does not include any studies with human participants or animals performed by any of the authors.

References

1. P.R. Woolcock, H. Tsai, in *Diseases of Poultry*, 13th edn., ed. by D.E. Swayne, J.R. Glisson, L.R. McDougald, L.K. Nolan, D.L. Suarez, V. Nair (John Wiley & Sons Inc, Ames, 2013), p. 422
2. P.P. Levine, J. Fabricant, *Cornell Vet.* **40**, 71 (1950)
3. S.A. Haider, B.W. Calnek, *Avian Dis.* **23**, 715 (1979)
4. R. Gough, M. Collins, E. Borland, L. Keymer, *Vet. Rec.* **114**, 279 (1984)
5. D. Todd, V.J. Smyth, N. Ball, B.M. Donnelly, M. Wylie, N.J. Knowles, B. Adair, *Avian Pathol.* **38**, 21 (2009)
6. T.E. Toth, *Avian Dis.* **13**, 834 (1969)
7. L. Wang, M. Pan, Y. Fu, D. Zhang, *Virus Genes* **37**, 52 (2008)
8. ICTV, The ICTV Online (10th) Report on Virus Taxonomy. (International Committee on Taxonomy of Viruses, 2017), <http://ictv.global/report>. Accessed 15 March 2017
9. C.H. Tseng, N.J. Knowles, H.J. Tsai, *Virus Res.* **123**, 190 (2007)
10. M. Soliman, M.M. Alfajaro, M.H. Lee, Y.J. Jeong, D.S. Kim, K.Y. Son, J. Kwon, J.S. Choi, J.S. Lim, J.S. Choi, *Arch. Virol.* **160**, 493 (2015)
11. A.M. Erfan, A.A. Selim, M.K. Moursi, S.A. Nasef, E. Abdelwhab, *Vet. Microbiol.* **177**, 347 (2015)
12. Y. Fu, M. Pan, X. Wang, Y. Xu, H. Yang, D. Zhang, *Vet. Microbiol.* **131**, 247 (2008)
13. J. Shi, X. Huang, Q. Liu, Z. Huang, *Vaccine* **31**, 2130 (2013)
14. J.Y. Cao, X.M. Ou, D.K. Zhu, G.P. Ma, A.C. Cheng, M.S. Wang, S. Chen, R.Y. Jia, M.F. Liu, K.F. Sun, *Virus Genes* **52**, 780 (2016)
15. Q.D. Cao, A.C. Cheng, M.S. Wang, *Rev. Med. Microbiol.* **23**, 18 (2012)
16. J. Kerkvliet, L. Papke, M. Rodriguez, *J. Virol.* **85**, 621 (2011)
17. R. Kumar, M. Hosamani, B.P. Sreenivasa, A. Kotyal, R. Venkataramanan, *Indian J. Virol.* **23**, 326 (2012)
18. S. Mahajan, J.K. Mohapatra, L.K. Pandey, G.K. Sharma, B. Pattnaik, *Biologicals* **43**, 47 (2015)
19. D. Paul, R. Bartenschlager, *World J. Virol.* **2**, 32 (2013)
20. S. Modrow, D. Falke, U. Truyen, H. Schätzl, in *Molecular Virology*, ed. by S. Modrow, D. Falke, U. Truyen, H. Schätzl (Springer, Berlin Heidelberg, 2013), p. 185
21. C.C. Kok, P.C. McMinn, *Int. J. Biochem. Cell Biol.* **41**, 498 (2009)
22. J. Lescar, B. Canard, *Curr. Opin. Struct. Biol.* **19**, 759 (2009)
23. M. Sierra, A. Airaksinen, C. González-López, R. Agudo, A. Arias, E. Domingo, *J. Virol.* **81**, 2012 (2007)
24. H.T. Nguyen, Y. Chong, D.K. Oh, Y.S. Heo, P.T. Viet, L.W. Kang, S.J. Jeon, D.E. Kim, *Anal. Biochem.* **434**, 284 (2013)
25. P. Gong, O.B. Peersen, *Proc. Natl. Acad. Sci. USA.* **107**, 22505 (2010)
26. L.L. Marcotte, A.B. Wass, D.W. Gohara, H.B. Pathak, J.J. Arnold, D.J. Filman, C.E. Cameron, J.M. Hogle, *J. Virol.* **81**, 3583 (2007)
27. G.S. Shatskaya, V.L. Drutsa, O.N. Koroleva, I.A. Osterman, T.M. Dmitrieva, *Biochem. Mosc.* **78**, 96 (2013)
28. M.C. Kim, Y.K. Kwon, S.J. Joh, A.M. Lindberg, J.H. Kwon, J.H. Kim, S.J. Kim, *J. Gen. Virol.* **87**, 3307 (2006)
29. Q.D. Cao, A.C. Cheng, M.S. Wang, *Adv. Mat. Res.* **647**, 396 (2013)
30. Q.D. Cao, A.C. Cheng, M.S. Wang, *Adv. Mat. Res.* **647**, 403 (2013)
31. M. Yang, A. Cheng, M. Wang, H. Xing, *J. Virol. Methods* **153**, 55 (2008)
32. M.C. Kim, Y.K. Kwon, S.J. Joh, J.H. Kwon, J.H. Kim, S.J. Kim, *Avian Dis.* **51**, 540 (2007)
33. C. Song, H. Wan, S. Yu, X. Han, X. Qiu, Q. Hu, L. Tan, C. Ding, *J. Virol. Methods* **182**, 76 (2012)

34. C.F. Li, Z.Y. Chen, C.C. Meng, G.Q. Liu, J. Virol. Methods **196**, 193 (2014)
35. A.C. Cheng, M.S. Wang, H.Y. Xin, D.K. Zhu, X.R. Li, H.J. Chen, R.Y. Jia, M. Yao, J. Microbiol. Methods **77**, 332 (2009)
36. H.A. El-Samadony, L.A. Tantawy, H.M. Mekky, Glob. Vet. **16**, 314 (2016)
37. Y.J. Wang, S.Y. Zhu, P.F. Cui, A.P. Wang, W.M. Hong, H. Lu, W.Y. Zuo, Afr. J. Microbiol. Res. **10**, 626 (2016)
38. N. González-Montalbán, E. García-Fruitós, A. Villaverde, Nat. Biotechnol. **25**, 718 (2007)
39. E.R. LaVallie, E.A. DiBlasio, S. Kovacic, K.L. Grant, P.F. Schendel, J.M. McCoy, Biotechnology **11**, 187 (1993)
40. G.L. Rosano, E.A. Ceccarelli, Front. Microbiol. **5**, 172 (2014)
41. L. García-Ortega, J. Lacadena, V. Lacadena, M. Masip, C. De Antonio, A. Martínez-Ruiz, A. Martínez del Pozo, Lett. Appl. Microbiol. **30**, 298 (2000)
42. E.R. LaVallie, Z. Lu, E.A. Diblasio-Smith, L.A. Collins-Racie, J.M. McCoy, Methods Enzymol. **326**, 322 (2000)
43. T. Akuta, T. Kikuchi-Ueda, K. Imaizumi, H. Oshikane, T. Nakaki, Y. Okada, S. Sultana, K. Kobayashi, N. Kiyokawa, Y. Ono, Protein Expr. Purif. **105**, 1 (2015)
44. A. Trabucchi, L.L. Guerra, N.I. Faccinetti, R.F. Iacono, E. Poskus, S.N. Valdez, Appl. Microbiol. Biotechnol. **94**, 1565 (2012)
45. Y. Li, Protein Expr. Purif. **81**, 201 (2012)
46. M. Askari, F. Gorjipour, Z. Sharifi, M.M. Farajollahi, Iran. J. Biotechnol. **10**, 249 (2012)
47. M.L. McNiff, E.P. Haynes, N. Dixit, F.P. Gao, J.S. Laurence, Protein Expr. Purif. **122**, 64 (2016)
48. H. Sonoda, Y. Kumada, T. Katsuda, H. Yamaji, Protein Expr. Purif. **70**, 248 (2010)
49. C. Bals, A. Schambach, J. Meyer, T. Scheper, U. Rinas, J. Biotechnol. **152**, 1 (2011)
50. S. Hartwig, T. Frister, S. Alemдар, Z. Li, U. Krings, R.G. Berger, T. Scheper, S. Beutel, Protein Expr. Purif. **97**, 61 (2014)
51. R.M. Brindeiro, M.A. Soares, A.B. Pacheco, O.H. de-Pontes, D.F. de-Almeida, A. Tanuri, Braz. J. Med. Biol. Res. **24**, 359 (1991)
52. J. Porath, Protein Expr. Purif. **3**, 263 (1992)
53. T. Cui, S. Sankar, A. Porter, J. Biol. Chem. **268**, 26093 (1993)
54. T. Cui, A.G. Porter, Nucleic Acids Res. **23**, 377 (1995)